Measurement Assisted Robotic Edge Deburring of Aero engine Components

NIROSH JAYAWEERA[1] and PHIL WEBB[2]
Department of Mechanical, Materials and Manufacturing Engineering[1]
University of Nottingham, UK.
nirosh.jayaweera@nottingham.ac.uk

Department of Systems Engineering and Human Factors[2]
University of Cranfield, UK.
p.f.webb@cranfield.ac.uk

Abstract: Aero engine components are often subjected to high stress levels and vibrations during operation. The mechanical integrity of these machined components may be compromised by the presence of burrs and sharp edges. Therefore the removal of burrs and the creation of rounded edges is necessary. To do this manually is time consuming and costly and may have potential quality issues. The application of robots to deburring has been limited by the difficulties in achieving the required degree of quality, controlling reaction forces during metal removal and the lack of tooling designed specifically for robots. The work presented in this paper introduces an efficient robotic deburring method, which is developed based on generation real-time robotic deburring path. The approach uses an in-process measurement sensor to determine the component's exact location prior to the deburring operation. The core of the system is a set of algorithms capable of fitting and generating the required robot path relative to the feature to be profiled. Reducing the reliance on accurate dedicated part holding fixtures and uses laser guided robot ensures the developed deburring system is highly flexible and re-configurable. The paper describes the development of deburring process for a simple straight edge feature and its application to more complex ones. The algorithms were evaluated using representative test pieces made from Titanium, RR1000 and super CMV alloys using a spindle attached to an industrial robot.

key-Words: aero-engine components, 'best-fit' algorithms, measurement assisted deburring, robotics, sensor

1 Introduction

The application of robotics to the deburring of aero engine components has been limited due to inconsistency of the burr formation, lack of real-time trajectory programming, the control systems applied to the robot, workpiece tolerances and inaccuracies in robot motion. Hence the majority of the existing deburring operations are performed manually with little use of CNC machines or robots. The manual method is time consuming, costly and demands a very high level of skill and experience to maintain consistency [1]. Most of these manual operations use hand held rotary tools that produce excessive vibration and may represent a health and safety risk coupled with potential errors that can damage expensive parts. CNC machines are attractive because of their stiffness and accuracy [2]. However, the cost of these machines is often too great for use in a deburring cell and they are inflexible due to the limited number of axes and range of motion. In contrast, robots are less stiff and accurate but offer larger work volumes and more controllable axes at a lower-cost than CNC machines [3][4].

Most conventional robotic deburring systems rely upon a simple pre-programmed path. The main disadvantage of this method is that it assumes that the part is perfect, located at a known position and the robot that travels along a rigid programmed path. This method shows inconsistencies in deburring due to slight misalignments between the work holding device and the robot as it follows its predefined path. This may either cause part of the burr to be left on the part edge or the tip of the cutting tool can be broken. For complex geometries, such as arcs and splines many points need to be taught along the surface for a robot to perform the trajectory accurately [5]. Therefore, the application of traditional teach programming for automating robotic deburring process is impractical when parts become complex and systems must have the capability to use CAD models to generate the necessary robot trajectories. However, the CAD model holds no information on the irregularities and thereby the path may not coincide exactly with the

shape or contour of the surface to be deburred because of variations in the part itself or differences between the part edge and the exact path the robot has interpolated. To overcome inaccuracies in robotic position, several control laws have been developed for simultaneous control of both motion and force to ensue that the cutting tool maintains contact with the workpiece at all times [6]. Much of the research involved in the area of control methods can be categorised into two major approaches: impedance control [7] and hybrid position/force control [8][9]. These methods require an accurate model of force interaction between the manipulator and the environment and are difficult to implement on typical industrial manipulators that are designed for position control.

The conventional force control method for the deburring process has the inherent characteristic of leaving the deburred surface as in imprint of the original and cannot distinguish the position deflection of the end-effector and larger burrs. To overcome this problem Wang et al. [10] proposed an impedance control method with an adaptive algorithm for the detection of burrs and cavities on a workpiece for the deburring process. In this approach impedance parameters can be modified by employing fuzzy control algorithms to improve force control performance and the velocity can be adjusted when the deburring tool encounters larger burrs and cavity defects. Schimmels [11][12] has presented a method for improving the positional capability and increasing the effective stiffness (bracing) of a robotic manipulator through multidirectional compliance and constraint. These mechanisms allow the robot to compensate for the excessive deflection when the robot contacts the workpiece. Kim et al.[13] developed a new active pneumatic tool based on a single pneumatic actuator with a passive chamber to provide compliance and reduce the chatter caused by air compressibility. In this active control scheme the actuators are commanded to increase torques in the opposite direction of the deflections. Liao et al. [14] presented a new approach for modeling and control of an automated deburring process that utilised a dual-purpose compliant toolhead which has a pneumatic spindle that can be extended and retract by three pneumatic actuators to provide tool compliance. Daniali and Vossssoughi [15] have developed an adaptive critic-based neurofuzzy controller to suppress the random vibration generation due to the interaction force end-effector and workpiece during the robotic deburring process. The majority of the work published on robotic deburring solutions either add compliance to the robot deburring tool or use force feedback devices either robot or robotic end-effector, the effectiveness of the developed methods is limited due to lack of flexibility.

The approach used here is to measure a number of points on the part to be deburred and use these to locally generate the robot path. This means that the robot can maintain a precise edge contour in spite of process errors such as robot inaccuracies, deviation in part geometry from the nominal and fixturing errors. The paper describes the development of the process for a simple straight edge feature and its application to more complex ones. The algorithms were evaluated using representative test pieces made from Titanium, RR1000 and super CMV alloys using a spindle attached to an industrial robot.

2 Methodology

The approach used here is to measure a number of points on the part to be deburred and use these to locally generate the robot path. The core of the system is a set of algorithms capable of fitting and generating the required robot path relative to the feature to be profiled. The advantage of this is that it minimises the setup requirements and eliminates the need for accurate features to provide datums, this is important since any features are likely to be indistinct due to the presence of burrs prior to the edge profiling process. An example of the methodology for a simple hole feature is presented below. An initial program that contains the approximate geometry of the part to be deburred is downloaded to the robot. It also contains a number of points at which the robot pauses and laser measurement system mounted on the robot end-effector is triggered and the offset of the edge from the robot Tool Center point (TCP) is obtained and stored. Since the sensor has two laser stripes it gives two measurements from a single position. For edge measurements, these are the x, y and z offset values from the intersection of the laser beams to the edge detected. As there are two beams, there are two points at which the edge is detected. The offset values are denoted as x1, y1, z1, x2, y2, z2. Once the path has been completed the offsets and robot positions are passed to a Matlab program as text files. The obtained data are then used to generate the actual geometry of the edges. Since burrs are present this will be uneven and displaced from the actual hard edge of the part. Performing a simple best fit relative to the measured geometry will tend to produce a path that is offset by the average size of

the burr. The method used in this application is a least-square fitting which is a mathematical procedure for finding the best-fitting circle to a given set of points. The obtained profile was further processed and filtered based on the expected geometry to compensate for the effect of the burrs on the edge profile. This corrected profile is then used to generate a new robot path. The generated deburring path is illustrated in Figure 1 as a schematic diagram.

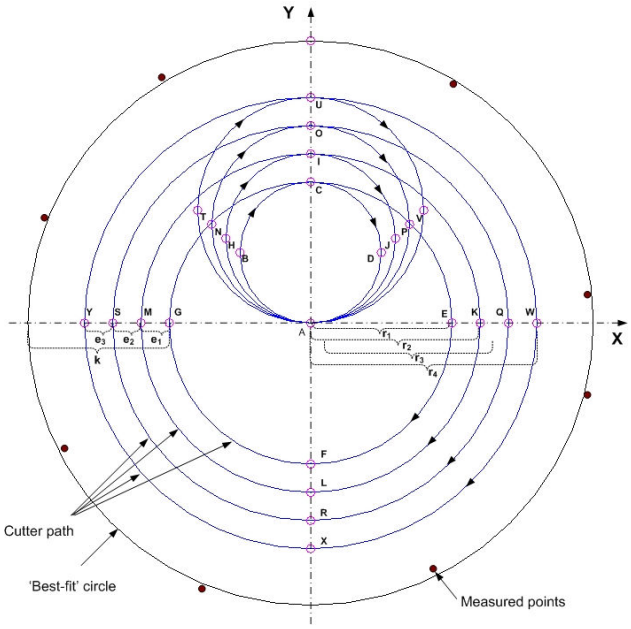

Fig. 1 Schematic diagram of cutting path generation

The notations used in the diagram are as follows:
Centre of the best-fit circle A = (x_0, y_0)
Radius of the best-fit circle = R
Cutting tool offset = k
Required Break Sharp Edge (e) can be defined as:

$$e = e_1 + e_2 + e_3 \qquad (1)$$

Where e1, e2 and e3 are the thickness of material removed by incremental passes of the cutting tool. Formulae for calculating radius of circles containing points CEFG, IKLM, OQRS and UWXY (r_1, r_2, r_3 and r_4) are:

$$r_1 = R - k \qquad (2)$$
$$r_2 = R - k + e1 \qquad (3)$$
$$r_3 = R - k + e_1 + e_2 \qquad (4)$$
$$r_4 = R - k + e_1 + e_2 + e_3 \qquad (5)$$

The point coordinates of C, E, F, G, I, K, L, M, O, Q, R, S, U, W, X and Y can be expressed as:

$$C = (x_0, y_0 + r_1); E = (x_0 + r_1, y_0)$$
$$F = (x_0, y_0 - r_1); G = (x_0 - r_1, y_0)$$
$$I = (x_0, y_0 + r_2); K = (x_0 + r_2, y_0)$$
$$L = (x_0, y_0 - r_2); M = (x_0 - r_2, y_0)$$
$$O = (x_0, y_0 + r_3); Q = (x_0 + r_3, y_0)$$
$$R = (x_0, y_0 - r_3); S = (x_0 - r_3, y_0)$$
$$U = (x_0, y_0 + r_4); W = (x_0 + r_4, y_0)$$
$$X = (x_0, y_0 - r_4);\ Y = (x_0 - r_4, y_0)$$

Formulae for calculating radius of circles containing points ABCD, AHIJ, ANOP and ATUV (u_1, u_2, u_3 and u_4) are:

$$u_1 = \frac{r_1}{2} \qquad (6)$$

$$u_2 = \frac{r_2}{2} \qquad (7)$$

$$u_3 = \frac{r_3}{2} \qquad (8)$$

$$u_4 = \frac{r_4}{2} \qquad (9)$$

The point coordinates of B, D, H, J, N, P, T and V can be expressed as:

$$B = (x_0 - u_1, y_0 + u_1); D = (x_0 + u_1, y_0 + u_1)$$
$$H = (x_0 - u_2, y_0 + u_2);\ J = (x_0 + u_2, y_0 + u_2)$$
$$N = (x_0 - u_3, y_0 + u_3);\ P = (x_0 + u_3, y_0 + u_3)$$
$$T = (x_0 - u_4, y_0 + u_4);\ V = (x_0 + u_4, y_0 + u_4)$$

The generated cutting tool path starts from point A followed by the trajectory represented by points B, C, E, F, G, C, D, A, H, I, K, L, M, I, J, A, N, O, Q, R, S, O, P, A, T, U, W, X, Y, U, V and A. Finally the data is transferred to the actual robot program to perform the deburring operation. The robot is programmed to perform a number of passes to incrementally remove any large burrs that may be present and also to minimise the cutting forces when the tool contacts the hard edge of the part.

The method described has a secondary advantage as it effectively performs a local calibration of the robot to the part meaning that the best possible performance is obtained. The approach developed also eliminates the need for precise location of the part in an expensive fixture and needs only simple low cost clamps to hold the workpiece.

3 Cell Construction

To prove the developed technologies a demonstrator cell was constructed which consisted of a Comau S4 robot, a purpose designed end-effector, PushCorp SM3002 spindle, Meta vision system, cutting and brushing tools, an overhead balanced cable carrier, testpiece and a modular fixture as shown in Figure 2. Care was taken when developing the cell to ensure that only generic 'off the shelf' systems were used to so that the resulting cell would be low cost and robust.

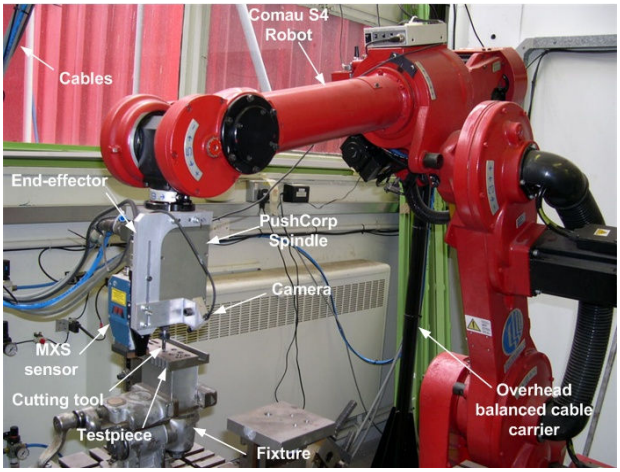

Fig.2 Experimental setup

The Comau S4 robot has an articulated, six axes anthropomorphic structure with a large working envelope. Its maximum wrist load capacity is 15 kg and electrical and pneumatic services are available at the forearm. The repeatability of this robot is ± 0.1 mm. The robot is controlled by an open version of the C3G controller unit with a communication link to a PC and PDL2 programming language is used to program the robot. The PushCorp SM3002 spindle is 3.6 kg in weight, 1.5 kW power, and has a 30,000 rpm top speed. The spindle utilises a manual ER series collets that has ability to clamp a wide range of tool shaft diameters. An overhead balanced cable carrier keeps the cables from becoming tangled in the robot. The servo cables, chilled water pipes and Meta sensor cable run through this system. The main components of the Meta vision system are the compact MXS sensor head, a control unit and a video monitor. The Meta MXS sensor uses two laser stripes to generate positional data on features of interest. The sensor control unit processes the picture from the camera and the software and uses the settings from the seam type to divide the stripe into lines that form that seam. From the position of the lines it can detect the location of the seam. Measurements from the picture are then converted into measurements in millimeters to give the seam's position under the sensor. The video monitor is needed during the installation of the system to allow the laser brightness to be adjusted correctly, and to verify that the sensor is getting a clear image from the part. Meta MXS cross sensor is a class 3B laser product and can be used to measure height, edge and hole finding applications. The purpose built end-effector enables the spindle, laser sensor and a camera to be mounted on the robot. The mathematical processing was performed using the Matlab software package running on a separate PC. A diagram of the cell resources and architecture is shown in Figure 3.

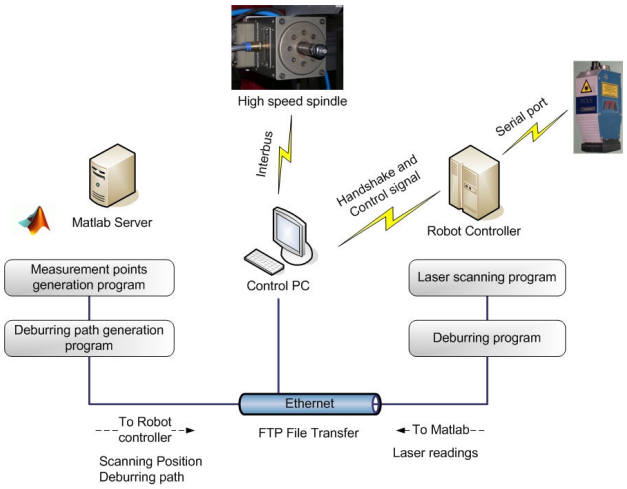

Fig. 3 Cell control architecture

Each of these elements has been integrated using Ethernet, interbus and serial communication. Ethernet was chosen due to its capability to support the transfer of large volumes of data through FTP file transfer protocols. An interbus based control module is fitted in the spindle cabinet and connected to the robot via an interbus cable. The unit produces an analogue voltage to control the velocity of the servo. A serial port was used to transfer the laser data to the robot controller, handshake between PC and robot controller and send control signals to the robot controller. This integrated system is capable of automatically passing data between all the system elements through a master PC running customised software developed by the University of Nottingham. The cell is controlled through a Graphical User Interface that allows and the operator to control and monitor all the operations and data flows within the system. It also provides error handling and diagnostic facilities. The process sequence used for the deburring of components is illustrated in Figure 4 as a flow chart.

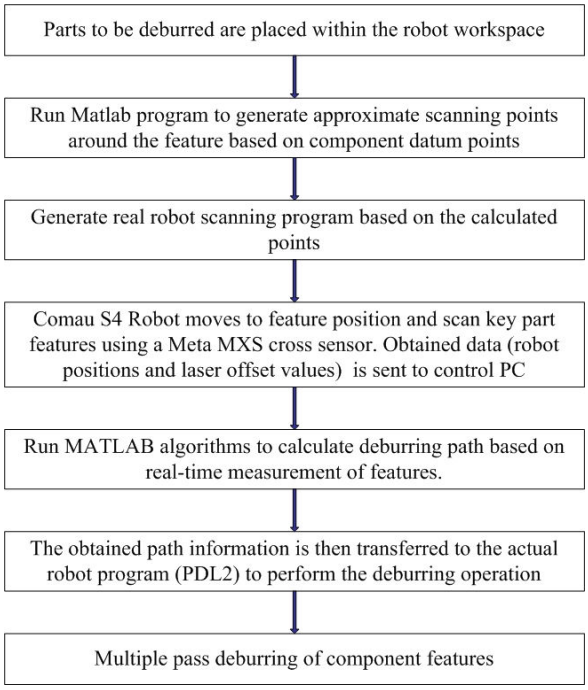

Fig. 4 Sequence of deburring procedure

4 System accuracy and repeatability

The accuracy of the robot can be defined as how closely the robot TCP can be programmed to hit a desired point [16][17]. Accuracy can be affected by both the speed of movement and the weight of the payload. The repeatability is concerned with the ability to position the TCP at a point in space that has previously been taught to the robot [18][19]. Good repeatability is more desirable than accuracy as inaccuracies are easier to correct. These especially true if the inaccuracies are consistent for all moves. If inaccuracy is consistent for all movements of robot, then the programmer can compensate for this error. Adjustment of poor repeatability is more difficult than consistent one. Repeatability can change with use, especially when robot performs the same task day after day. This is because mechanical components are subject to wear, thus increasing mechanical inaccuracies, this reduces the repeatability.

4.1 Robot accuracy

This experiment was set up to evaluate the robot accuracy. Experiments were carried out to analyse the robot measured distance against the actual distance travelled to quantify robot error compared with the measured distance. This was done using a Renishaw ML10 laser measurement system. The ML10 is an "eyes safe" Class II low power Helium-Neon laser with a wavelength of 632.9 nm and nanometer resolution. The unit contains the laser tube, power supply, stabilisation circuitry, optical detector and detection computation circuitry, including the fringe counter, interpolation and signal strength function. The experimental setup is shown in Figure 5. Experiments were performed for each of the robot's three Cartesian coordinate axes and the obtained results are presented in Table 1. Figure 6 graphically represents the robot accuracy along each of the axes.

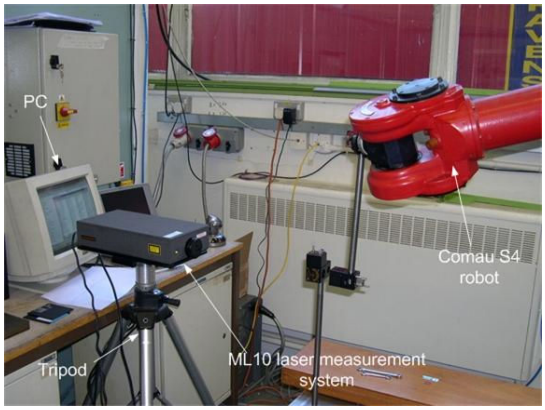

Fig. 5 Experimental setup for robot accuracy measurements

Distance (mm)	X error (mm)	Y error (mm)	Z error (mm)
0	0.0156	0.0015	-0.0014
50	-0.2772	-0.1547	0.4586
100	-0.5496	0.0084	1.0536
150	-0.7368	-0.0995	1.3591
200	-0.9166	-0.2556	1.6477
250	-0.9111	-0.3023	1.8848
300	-0.9462	-0.3099	2.0697
350	-0.9417	-0.5671	2.2083
400	-0.8923	-0.7112	2.2702
450	-0.612	-0.885	2.4548
500	-0.5348	-1.1254	2.4837
550	-0.4371	-1.1586	2.5321
600	-0.3125	-1.417	2.5783
650	-0.1024	-1.6061	2.4699
700	0.1654	-1.8969	2.4309
750	0.4394	-2.1045	-
800	0.7623	-2.2923	-
850	-	-2.4959	-

Table 1 Robot accuracy measurements

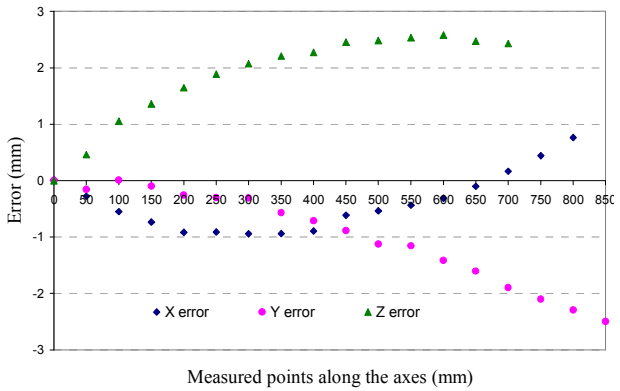

Fig. 6 Experimental setup for robot accuracy measurements

It can be seen from the graph that the accuracy of S4 robot is ±2.58mm. The robot used was fairly old and significant backlash was found during the experiments.

4.2 Robot repeatability

This experiment was performed to analyse the robot repeatability. This experiment robot was repeatedly moved a known distance defined by a length gauge, and a dial gauge used to measure any deviation. This experiment was carried out for different length gauges (145mm, 525mm, 725mm, and 1025mm) and the obtained results are shown in Table 2.

Experimental trials	Dial gauge readings for different length gauges			
	145mm	525mm	725mm	1025mm
1	0.0229	-0.0030	-0.0127	0.0356
2	0.0178	-0.0380	-0.0254	-0.0026
3	0.0280	-0.0230	0.0432	0.0026
4	0.0254	-0.0410	0.0229	0.0381
5	0.0254	-0.0380	0.0229	0.0356
6	0.0229	-0.0480	-0.0254	0.0381
7	0.0203	-0.0480	-0.0229	0.0254
8	0.0127	-0.0480	-0.0229	0.0356
9	0.0178	-0.0510	-0.0254	0.0305
10	0.0203	-0.0510	-0.0254	0.0305

Table 2 Robot repeatability measurements

Therefore the worst case robot positional repeatability for the obtained data was 0.068 mm. The results indicate that the Comau S4 robot repeatability is consistent and within the manufacturer's quoted repeatability of ± 0.1 mm.

The individual sources of error can be combined to give an estimate of the overall system error. The magnitudes of the empirically obtained accuracies for the system components are show below:
Robot positional accuracy $PA_{Robot} = \pm 0.1$ mm
Horizontal measurement accuracy of the sensor head (PA_{Sensor}) = ± 0.08 mm
Vertical measurement accuracy of the sensor head (PA_{Sensor}) = ± 0.02 mm
The total system positional accuracy (PA_{System}) can then be calculated from:

$$PA_{System} = \pm\sqrt{PA_{Robot}^{\ 2} + \ PA_{Sensor}^{\ 2}} \qquad (10)$$

Therefore, the system measured positional accuracies are:
In the horizontal plane = ± 0.128 mm
In the vertical plane = ± 0.102 mm

5 Cell testing and evaluation

To verify the capability of developed system two separate sets of experimental trials were conducted to evaluate the baseline capability of the cell and its ability to perform edge breaking on more complex (circular) features.

5.1 Deburring of straight edges

This experiment was setup to investigate the influence on the finish of the profiled edges with varying spindle speed and feed rates.

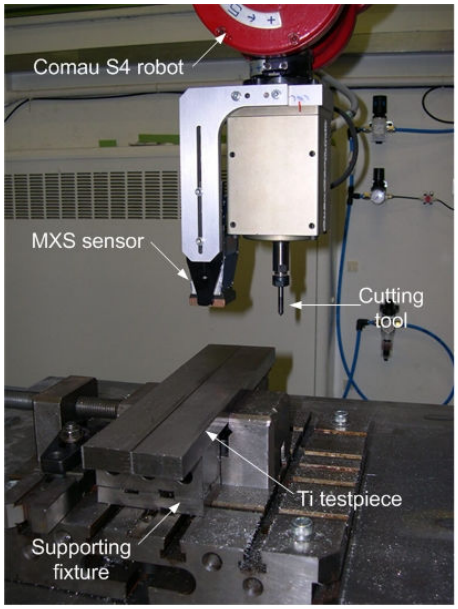

Fig. 7 Experimental setup for deburring trials on Ti testpiece

Following the edge profiling tests, further practical work was undertaken on the samples to assess the brushing operation. The first set of experiments was carried out using just the robot and spindle to evaluate the base performance of the cell as shown in Figure 7.

The test component used within the experiment was manufactured from Ti64 with 'as machined' sharp edges. The size of the burrs was variable and typically a few millimeters with a thickness of 0.1 – 1.0 mm. The components were clamped in to the cell and the component's edge positions measured relative to the robot's coordinate system. Then a simple cutting path is run with the spindle running parallel to the edge of the part. The experiment was performed several times with a different set of cutting parameters in each case. Normally, the burrs are rough edges which are generated as a result of machining processes. These burrs are called primary burrs. During the deburring process, secondary burrs are generated due to slight removal of material as shown in Figure 8. To remove these secondary burrs brushing is performed as shown in Figure 9.

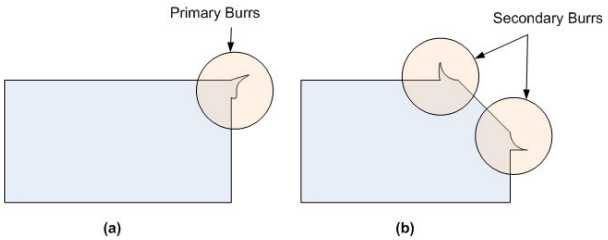

Fig. 8 Burr formation (a) Primary burrs (b) Secondary burrs

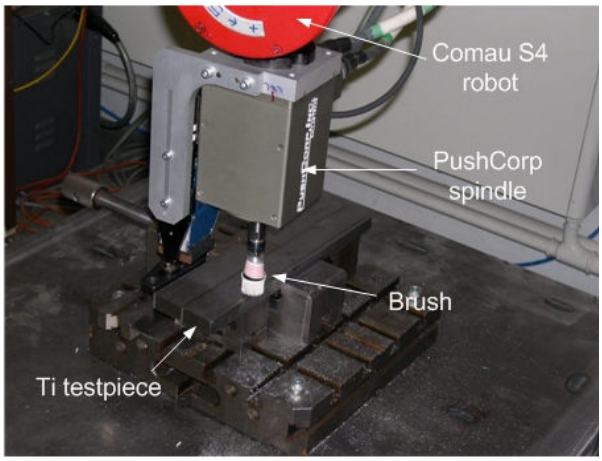

Fig. 9 Experimental setup for brushing trials on Ti testpiece

The effect of the brush is to remove the tops of any peaks without changing core roughness. Hence, brushes can refine surface finishes produce by deburring operations. Following the deburring process the edges were brushed using a rotating brush mounted on the spindle. Three brushing trials were performed for each edge to remove secondary burrs and brushing orientations are illustrated in Figure 10.

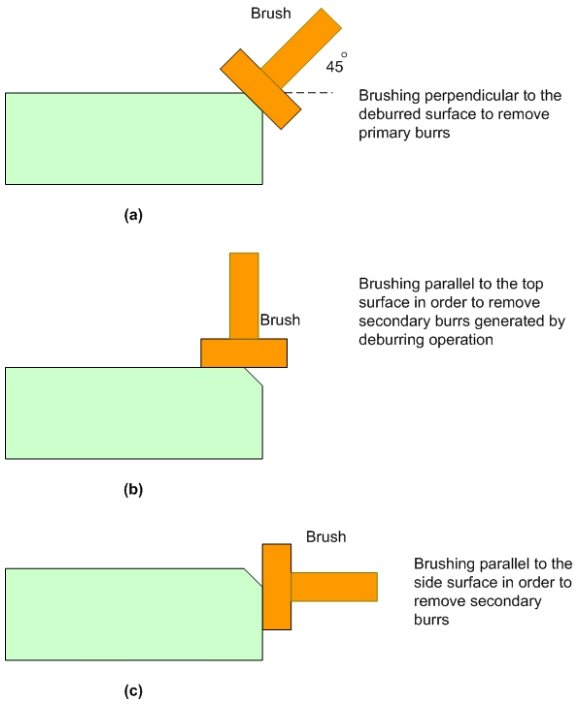

Fig. 10 Brushing orientations for removing primary and secondary burrs

Figure 11 shows the shows a micrograph of the profiled edges of the titanium test pieces.

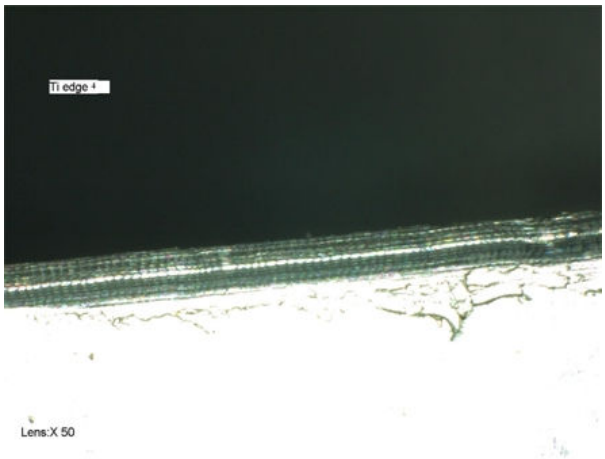

Fig. 11 Micrograph of profiled edge of Ti testpiece

The micrographs were captured using a Keyence VHX-100 Video Digital Microscope. These micrographs also indicated that the robot exhibited slight chatter during deburring operations. . A micrograph of a deburred and brushed edge of a Titanium test piece is shown in Figure 12.

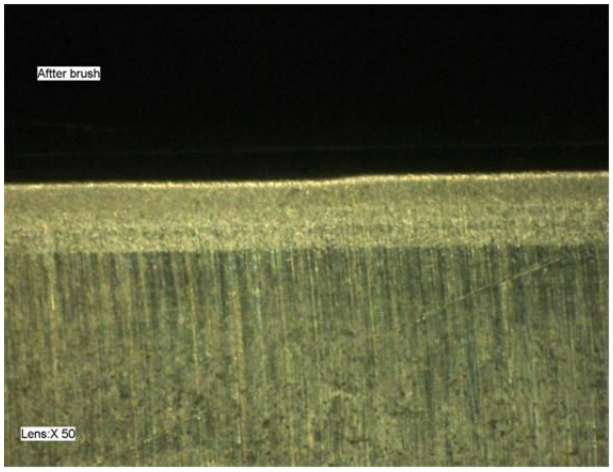

Fig. 12 Micrograph of Ti testpiece after brushing trials

After machining the profiled edges were measured for surface roughness (Ra value) using a FOGALE nanotech non-contact PHOTOMAP 3D machine. The measured Ra values with relevant deburring parameters are presented in Table 3. Profiled edges are shown in Figure 13.

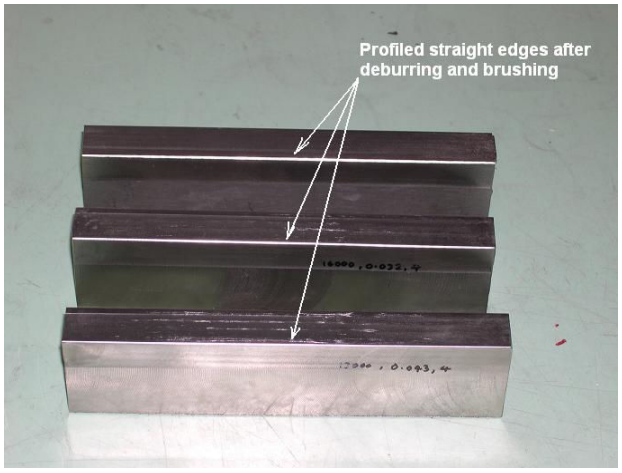

Fig.13 Profiled straight edges after deburring and brushing trials

Spindle Speed (rpm)	Feed rate (m/s)	Feed/tooth (mm/tooth)	Ave Ra (μm)
13000	0.026	0.03	0.983
13000	0.043	0.05	0.732
16000	0.032	0.03	0.968
16000	0.053	0.05	1.010
18000	0.036	0.03	0.793
18000	0.060	0.05	0.957

Table 3 High speed deburring and brushing trials for Titanium test pieces

The obtained results for straight edge deburring and brushing trials for titanium test pieces showed promising results and surface finishes were close to the typical standard set by the aerospace industry of 0.8 Ra value. Figure 14 shows the tool wear and damage during edge proofing operation without coolant.

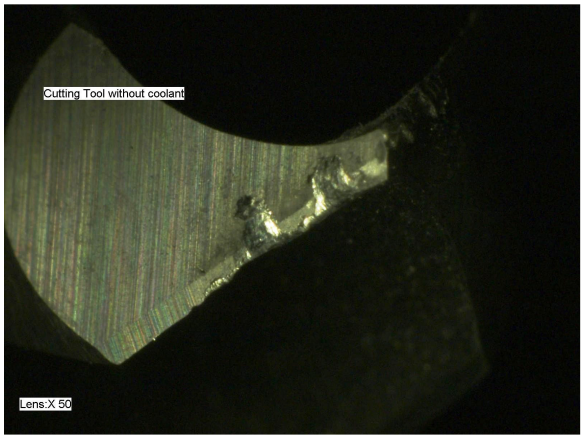

Fig. 14 Micrograph of tool damage after edge profiling of Ti testpiece

5.2 Deburring of Circular Feature

A series of experimental trials were performed on a test piece to analyse the feasibility of robotic deburring of circular features. The testpiece consisted of a number of representative features that can be found in aero-engine components. Representative features include small circular holes, edges, stepped holes, slots, and straight and curved tooth profiles. This paper describes the experimental trials were performed for deburring of circular features. The testpiece used was in the 'as machined' condition with burrs present on the part features. Three different test pieces were used manufactured from Titanium64, Super CMV and RR1000. Experiments were performed each following the operation procedure described in Figure 4 and methodology used to calculate circular

holes described in methodology section. An example of holes with burrs and deburred holes on a RR1000 testpiece is shown in Figure 15. Figure 16 shows a micrograph of profiled circular feature on RR1000 testpiece.

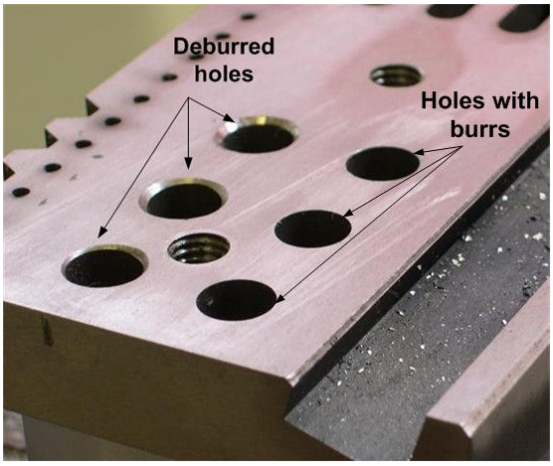

Fig. 15 A photograph of holes with burrs and deburred holes on RR1000 test piece

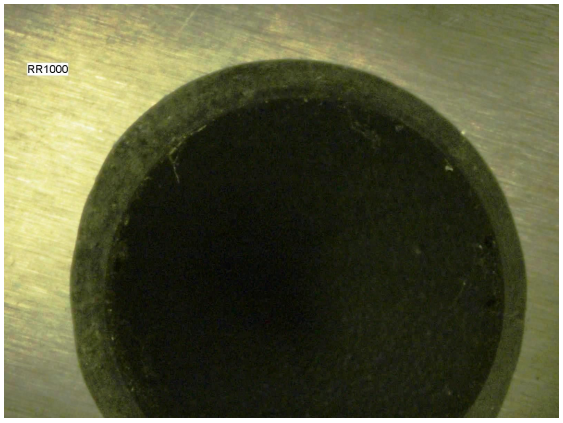

Fig. 16 A micrograph of deburred hole on RR1000 testpiece

The measured surface roughness values, Ra of profiled circular feature for different materials (Super CMV, Ti6Al4V, and RR1000) are presented with relevant deburring parameters in Table 4.

Spindle Speed (rpm)	Feed rate (m/s)	Material	Ave Ra (μm)
8000	0.0025	Super CMV	3.25
8000	0.0025	Super CMV	2.97
8000	0.0025	Super CMV	3.10
8000	0.0025	Ti6Al4V	2.90
8000	0.0025	Ti6Al4V	3.17
8000	0.0025	Ti6Al4V	3.24
8000	0.0025	RR1000	3.95
8000	0.0025	RR1000	3.30
8000	0.0025	RR1000	3.35

Table 4 Surface roughness measurements of circular feature on different materials

According to experimental results, the developed system is capable of bringing down the geometric inaccuracy to less than ± 0.3 mm which is slightly higher than the standard set by the aerospace industry of ± 0.2 mm. The geometrical accuracy is dependent on burr presence and the geometrical accuracy of the feature. The surface roughness values obtained are higher than the typical standard set by the aerospace industry of 0.8 μm. However, these experiments were performed without coolant and brushing operations and the deburring parameters used were not optimal. From the results obtained from the experiments two problems were identified. They were surface roughness and chatter. Heat generation during metal cutting affects both the material and the tool life. Increases in temperature can weaken tool strength locally and increase wear and cause metallurgical phase changes at the tool surface [20]. Therefore it is proposed that the surface finish can be improved by using a cutting fluid on deburring. Workpiece tolerances and robotic inaccuracies make it difficult for the deburring tool to maintain the constant force needed to cut an even chamfer across a workpiece. Due to backlash and the stiffness of the robot the cutting tool may bounce in and out of the workpiece during the deburring operation and cause chattering, which may contribute to produce an uneven chamfer and diminishes the quality of the deburring operation. The developed methodology is generic and has been successfully applied for the deburring of circular features on Trent 900 high pressure compressor disc.

6 Conclusion

This research has successfully proved the feasibility of robotic deburring of aero-engine components using automated path generation. The initial deburring and brushing trials for the titanium test pieces showed promising results and the results were close to the typical standard set by the aerospace industry of 0.8 Ra value. It is proposed that by using a stiffer robot and using cutting fluid the surface finish can be significantly improved. The incorporation of an MXS sensor and mathematical algorithms allowed precision chamfers to be generated in spite of part tolerances, fixturing errors and robot positional accuracy. The approach developed also eliminates the need for precise location of the part in an expensive fixture and needs only simple low cost clamps to hold the workpiece. The developed methodology can be further applied for more complex feature deburring applications.

Acknowledgement

This work was funded by Rolls-Royce PLC.

References:

[1] Valente, C., Oliveira, J., A new approach for tool path control in robotic deburring operations, ABCM Symposium series in Mechatronics, Vol. 1, 2004, pp. 124-133.
[2] Bogue, R., Finishing robots: a review of technologies and applications, Industrial Robot, Vol. 36, No.1, 2009, pp 6–12.
[3] Kim, C. and Chung, J., Robust Coordination Control of a Pneumatic Deburring Tool, Journal of Robotic Systems, 22 (Supplement), 2006, S1-S13.
[4] Roebrock, P., A flexible multi-sensor positioning system for industrial robots, WSEAS Transactions on Electronics, Issue 3, Vol. 5, 2008, pp. 93-100.
[5] Stouffer, K., Michaloski, J., Russell, B., Proctor, F.M., ADACS - An Automated System for Part Finishing, Proceedings of International Conference on Industrial Electronics, Control, Instrumentation and Automation (IECON), 1993, pp. 581-586.
[6] Zhang, H., Chen, H., Xi, N., Zhang, G., He, J., On-line path generation for robotic deburring of cast aluminium wheels, IEEE/RSJ international conference on intelligent robots and systems, Beijing, China, 2006, pp. 2400-2405.
[7] Wang, X., Wang, Y., Xue, Y., An adaptive algorithm for robotic deburring based on impedance control, IEEE international symposium on industrial electronics, Montreal, Quebec, Canada, 2006, pp. 262-266.
[8] Pires, J., Afonso, G., Force control experiments for industrial applications: a test case using an industrial deburring example, Assembly Automation, Vol. 27, No. 2, 2007, pp. 148-156.
[9] Ziliani, G., Visioli, A., Legnani, G., A mechatronic approach for robotic deburring, Mechatronics, Vol. 17, 2007, pp.431–441.
[10] Wang, X., Wang, Y., Xue, Y., Adaptive Control of Robotic Deburring Process Based on Impedance Control, IEEE International Conference on Industrial Informatics, Singapore, 2006, pp 921-925.
[11] Schimmels, J., Multidirectional compliance and constraint for improved robotic deburring.Part 1: improved positioning, Robotics and Computer Integrated Manufacturing, Vol.17, 2001, pp. 277-286.
[12] Schimmels, J., Multidirectional compliance and constraint for improved robotic deburring.Part 2: improved bracing, Robotics and Computer Integrated Manufacturing, Vol. 17, 2001, pp. 287-294
[13] Kim, C., Chung, J., Hong, D., Coordination control of an active pneumatic deburring tool, Robotics and computer integrated Manufacturing, Vol. 24, 2008, pp 462-471.
[14] Liao, L., Xi, F., Liu, K., Modeling and control of automated polishing/deburring process using a dual-purpose compliant toolhead, International journal of Machine Tools & Manufacture, Vol. 48, 2008, pp. 1454-1463.
[15] Daniali, M., Vossoughi, G., Intelligent active vibration control of constrained manipulator in robotic deburring, International conference on Industrial Mechatronics and Automation, Chengdu, China, 2009, pp. 76-80.
[16] Kleinkes, M., Neddermeyer, W., Schnell, M., An automated quick accuracy and output signal check for industrial robots, Proceedings of the 6th WSEAS International Conference on Robotics, Control and Manufacturing Technology, Hangzhou, China, April 16-18, 2006, pp. 232-237.
[17] Niola, V., Rossi, C., Savino, S., A Robot Cinematic Calibration Technique, Proceedings of the 5th WSEAS Int. Conf. on Signal Processing, Robotics and Automation, Madrid, Spain, February 15-17, 2006, pp. 82-86.
[18] Torabian, H., Mohammadion, A., Design and Construction of Multi Axes Data Acquisition System for Robot performance Measurement, Proceedings of the 6th WSEAS International Conference on Signal Processing, Robotics and Automation, Corfu Island, Greece, February 16-19, 2007, pp. 158-163.
[19] Ismail, A., Hassan, A., Syamsuddin, S., Nuawi, M., Abdullah, S., Ibrahim, H., The Repeatability Analysis of Industrial Robot under Loaded Conditions and Various Distances, 8th WSEAS Int. Conf. on Robotics, Control and Manufacturing Technology, Hangzhou, China, April 6-8, 2008, pp. 75-79.
[20] Nuawi, M., Nor, M., lamin, F., Abdullah, S., Nizwan, C., Tool Life Monitoring using Coefficient of Integrated Kurtosis-based Algorithm for Z-filter (I-kaz) Technique, Proceedings of the 7th WSEAS International Conference on Wavelet Analysis & Multirate Systems, Arcachon, France, October 13-15, 2007, pp. 142-146.